Optical-model partial-wave analyses of p-^{4}He elastic scattering*

L. G. Arnold and B. C. Clark
Department of Physics, The Ohio State University, Columbus, Ohio 43210

R. L. Mercer
Speech Processing Group, Computer Sciences Department, International Business Machines Corporation, Thomas J. Watson Research Center, Yorktown Heights, New York 10598

D. G. Ravenhall
Physics Department, University of Illinois, Urbana, Illinois 61801

A. M. Saperstein
Department of Physics, Wayne State University, Detroit, Michigan 48202
(Received 28 July 1975)

We have performed optical-model calculations using the Klein-Gordon and the Dirac equations for the 600 MeV p-^{4}He scattering experiments of Boschitz *et al.*, and the 1050 MeV p-^{4}He scattering experiments of Baker *et al.* We have compared these analyses with our previous analysis of the 1000 MeV p-^{4}He experiment of Palevsky *et al.* In comparing the results at the three energies we find that the experiments require a slightly energy-dependent optical potential rms radius. The average value is in good agreement with the ^{4}He matter radius obtained from electron scattering, and substantially smaller than the low energy ^{4}He optical potential rms radius. On the other hand, the experiments require quite different values for the optical potential strength parameters.

[NUCLEAR REACTIONS ^{4}He(p,p) $E=600$, 1000, 1050 MeV, $\sigma(\theta)$ calculated, deduced optical-model parameters.]

INTRODUCTION

Elastic differential cross sections are available for the scattering of 600,[1] 1000,[2] and most recently 1050[3] MeV protons from ^{4}He. We present here the results of an optical-model analysis of the 600 and 1050 MeV cross sections. Together with our earlier analysis of the 1000 MeV results,[4] we are able to comment on the energy dependence of some optical-model parameters, and to examine the consistency of the two sets of results around 1000 MeV.

The optical potential used in this work has the form

$$U=(V+iW)f(r)\ . \tag{1}$$

In most of our calculations the shape function $f(r)$ is chosen to have the same functional form as the charge distribution determined from electron scattering experiments. At the energies we consider, one expects relativistic effects to be important, therefore we have used both the Klein-Gordon and Dirac equations in our calculations. As we use relativistic wave equations, the transformation characteristic of the potential must be considered. We have chosen the potential of Eq. (1) to be either a Lorentz-scalar potential U_s or the fourth component of a four-vector potential U_4. The three-vector part of the four-vector is assumed to be zero. The Klein-Gordon equation is then

$$[\nabla^2+[E-(U_4+V_C)]^2-(m+U_s)^2]\,\phi_{KG}(\vec{r})=0\ , \tag{2}$$

and the four-component Dirac equation is

$$\left[\begin{pmatrix}0 & \vec{p}\cdot\vec{\sigma}\\ \vec{p}\cdot\vec{\sigma} & 0\end{pmatrix}+\begin{pmatrix}(m+U_s) & 0\\ 0 & -(m+U_s)\end{pmatrix}-\begin{pmatrix}E-(U_4+V_C) & 0\\ 0 & E-(U_4+V_C)\end{pmatrix}\right]\phi_D(\vec{r})=0\ . \tag{3}$$

Here V_C is the Coulomb potential obtained from the charge distribution of the nucleus, $E^2=p^2+m^2$, and m is the proton rest mass. We have shown previously[4] that as long as the transformation character of the potential is pure U_s or pure U_4 the Klein-Gordon and Dirac equations yield essentially identical cross sections. Thus, under these conditions, the effect of the nucleon spin is small for calculations with a spin-independent potential. The separate question of the spin dependence of the potential is not considered in our analysis. We point out, however, that the results of several recent

TABLE I. Results of the Watson model calculations for a U_4 type potential. The shapes A, B, and C are defined in the text. The potential strengths V and W are obtained from the averaged two-nucleon scattering amplitude.

T (MeV)	Shape	V (MeV)	W (MeV)	$\|t\| \leq 0.2$ (GeV/c)^2 χ^2/d.f.	λ	$\|t\| \leq 0.4$ (GeV/c)^2 χ^2/d.f.	λ	All data χ^2/d.f.	λ	J/A (MeV fm^3)	σ_R (mb)	$\langle r^2 \rangle^{1/2}$ (fm)
587	A	25.28	−58.78	3.84	1.21	12.12	1.26	22.57	1.29	113.0	89.7	1.63
587	B	25.92	−60.27	2.59	1.19	5.86	1.24	18.62	1.27	113.0	87.9	1.67
587	C	26.90	−62.56	3.43	1.22	11.07	1.27	22.70	1.29	113.0	90.9	1.72
1000	A	15.12	−75.60	3.41	1.56	15.30	1.51	18.96	1.43	67.6	97.3	1.63
1000	B	15.50	−77.51	2.45	1.45	6.50	1.44	12.61	1.39	67.6	95.2	1.67
1000	C	16.09	−80.45	3.34	1.56	14.60	1.51	19.06	1.43	67.6	98.6	1.72
1050	A	15.28	−76.38	8.47	1.51	67.34	1.88	61.64	2.10	68.3	97.3	1.63
1050	B	15.66	−78.31	7.28	1.47	21.24	1.75	44.16	1.91	68.3	95.2	1.67
1050	C	16.26	−81.28	7.20	1.50	61.56	1.87	64.40	2.11	68.3	98.7	1.72

analyses of intermediate energy p-^{4}He scattering indicate that spin-dependent effects yield small corrections to the elastic cross section.[5–7] Thus, observations regarding the central optical potential obtained in this work are not likely to be altered very much by inclusion of a spin-dependent potential.

In analyses of low energy (≤ 50 MeV) nucleon-nucleus elastic scattering data, Greenlees, Pyle, and Tang[8] have found that characteristic properties of the optical model which are well determined by experiment are the volume integral and rms radius of the real part of the central potential. Van Oers *et al.*[9] have extended these analyses to higher energies in an effort to map out the energy dependence of the volume integral per nucleon. Our results from considering each of the three experiments separately also indicate that the rms radius and volume integral are well determined by the data. Further, the rms radii obtained from the fits at the different energies agree to within 15%, and exhibit a tendency to increase slightly with energy. We can make no statement, however, regarding the energy dependence of the volume integral per nucleon J/A, since the Brookhaven data at 1000 MeV and the Saclay data at 1050 MeV predict substantially different values for this quantity.

CALCULATIONS AND RESULTS

The starting point for our analysis of p-^{4}He elastic scattering is a simple form of the Watson optical potential given by

$$U = -\frac{A\sigma_T k}{2E}(i+\alpha)\rho(r)\ , \tag{4}$$

where A is the number of nucleons in the target, α is the ratio of real to imaginary parts of the nucleon-nucleon forward scattering amplitude, σ_T is the average nucleon-nucleon total cross section, k and E are the projectile momentum and total energy taken in the nucleon-nucleus center of mass system. This form of the optical potential is used for the fourth component of a four-vector potential. The corresponding scalar Watson potential is obtained from the prescription $U_s = (E/m)U_4$. The density $\rho(r)$ is taken to the charge density determined from electron scattering, a common approximation that is succinctly described by Feshbach, Gal, and Hüfner.[10] The charge density is normalized to unity.

There are several forms for the ^{4}He charge density given in the literature. Frosch *et al.*[11] found that a modified Gaussian form factor given by

$$F(q) = [1 - (a^2q^2)^n]e^{-b^2q^2} \tag{5}$$

TABLE II. Results of the Watson model calculation for a Lorentz-scalar potential with shape C. The potential strengths are obtained by an E/m scaling of the vector potential strengths.

T (MeV)	V (MeV)	W (MeV)	$\|t\| \leq 0.2$ (GeV/c)^2 χ^2/d.f.	λ	$\|t\| \leq 0.4$ (GeV/c)^2 χ^2/d.f.	λ	All data χ^2/d.f.	λ	J/A (MeV fm^3)	σ_R (mb)
587	36.82	−85.63	3.15	1.21	9.59	1.26	20.65	1.30	154.7	91.8
1000	25.71	−128.56	3.19	1.54	13.34	1.50	17.46	1.43	108.0	99.3
1050	26.41	−132.07	6.64	1.49	52.42	1.88	53.35	2.10	111.0	99.4

TABLE III. Results of two-parameter fits to the experimental cross sections for a U_4 potential with shapes A and C. The strength parameters V and W were varied to obtain a best fit for $|t| \leq 0.2$ (GeV/c)^2.

T (MeV)	Shape	V (MeV)	W (MeV)	$\|t\| \leq 0.2$ (GeV/c)^2 χ^2/d.f.	λ	$\|t\| \leq 0.4$ (GeV/c)^2 χ^2/d.f.	λ	All data χ^2/d.f.	λ	J/A (MeV fm^3)	σ_R (mb)
587	A	50.66	−45.05	0.87	0.97	3.28	0.96	14.30	1.03	220.9	72.3
587	C	53.89	−47.36	1.75	0.98	6.22	0.98	17.02	1.05	226.4	74.5
1000	A	49.55	−90.08	0.95	1.11	13.01	0.98	10.23	1.11	216.1	101.2
1000	C	48.93	−96.39	1.69	1.22	11.93	1.14	11.03	1.18	205.6	107.5
1050	A	64.56	−88.91	2.05	1.02	11.18	0.73	33.72	0.85	281.6	99.3
1050	C	68.57	−100.73	2.77	1.06	11.39	0.89	25.74	1.03	288.0	108.6

with $n = 6$, $a = 0.316$ fm, and $b = 0.681$ fm gives a good representation of the experimental electron scattering form factors. The density obtained from the Fourier transform of Eq. (5) has an rms radius of 1.67 fm. We refer to this as density A. Frank, Haas, and Prange[12] have determined an rms charge radius of 1.63 ± 0.04 fm from low energy electron scattering. Frank *et al.* give no functional form for $\rho(r)$ so we chose for the remaining charge densities a parabolic Fermi shape,

$$\rho(r) = \frac{1 + wr^2/c^2}{1 + \exp[(r-c)/z]} . \tag{6}$$

For density B we use a Fermi shape, $w = 0$, and take $z = 0.33$ fm in order to have the same skin thickness as density A. The rms radius of 1.63 fm then fixes c to be 1.387 fm. Finally, for density C, we use the form given by Eq. (6) with the parameters determined by Frosch *et al.* from electron scattering. These parameters are $c = 1.008$ fm, $z = 0.327$ fm, and $w = 0.445$, yielding an rms radius of 1.72 fm.

In this first comparison, the remaining parameters of Watson model potential Eq. (4) are taken from the literature. For the 600 MeV experiments we took $\sigma_T = 39$ mb and $\alpha = -0.43$. These values were used in the Glauber calculations of Ref. 1. For the 1000 and 1050 MeV experiments we used $\sigma_T = 43.91$ mb[13] and $\alpha = -0.2$.[14] We now discuss the Watson model calculations using densities A, B, and C.

The Watson model of Eq. (4) is expected to be best for small angle scattering. We have, therefore, fitted the data at each energy over three ranges of recoil momentum squared, $|t|$ measured in (GeV/c)^2. First we consider data before the first diffraction dip, $|t| \leq 0.2$, then we extend the fitting to $|t| \leq 0.4$, which includes the dip and subsequent maximum, and then we finally fit all of the data. As in our previous work,[4] we calculate both the relative χ^2 per degree of freedom (d.f.) and a parameter λ which is a measure of the overall goodness of fit to the absolute cross section.[15] The results are given in Table I, and the differential cross sections for density C are shown as the dashed curves in Figs. 1 and 2; the corresponding results for 1000 MeV are shown in Fig. 1 of Ref. 4. As would be expected, the χ^2/d.f. increases as the fits are extended to larger angles. The quality of the Watson model fits is not good even at the smallest angles; however, the shape with the smallest rms radius produces the best fit at each energy. A scalar potential obtained from the E/m scaling of Eq. (4) does not produce significantly different results, as is shown for density C in Table II.

As the values of α and σ_T are not well known, the next step in our calculations is to see if a good fit to the data can be found using the charge distribution for $f(r)$ and allowing V and W, or equivalently σ_T and α, to vary. The parameter searches on V and W were performed using densities A and C, and the results are given in Tables III and IV. As the Watson model is expected to be best for small angles, we first search on V and W using

TABLE IV. Results of two-parameter fits to the experimental cross sections for a U_4 potential with shape A. The strength parameters V and W were varied to obtain a best fit to all data.

T (MeV)	V (MeV)	W (MeV)	$\|t\| \leq 0.2$ (GeV/c)^2 χ^2/d.f.	λ	$\|t\| \leq 0.4$ (GeV/c)^2 χ^2/d.f.	λ	All data χ^2/d.f.	λ	J/A (MeV fm^3)	σ_R (mb)
587	52.02	−49.78	0.87	0.94	3.27	0.92	13.97	0.99	226.8	76.5
1000	33.14	−91.04	1.21	1.23	3.57	1.19	7.47	1.21	144.5	102.7
1050	47.11	−71.05	2.27	1.22	2.62	1.29	19.68	1.45	205.5	88.6

TABLE V. Results of three-parameter fits to the experimental cross sections. A parabolic Fermi shape was used with $c = 1.008$ fm and $w = 0.445$. The parameters z, V, and W were varied. Of the two U_s entries at each energy, the first gives the results of an E/m scaling of the U_4 potential and the second is an independent fit. The last entry in the table gives the results of a calculation at 1050 MeV using the U_4 potential from 1000 MeV.

T (MeV)	Type	z (fm)	V (MeV)	W (MeV)	$\|t\| \leq 0.2$ (GeV/c)^2 χ^2/d.f.	λ	$\|t\| \leq 0.4$ (GeV/c)^2 χ^2/d.f.	λ	All data χ^2/d.f.	λ	$\langle r^2 \rangle^{1/2}$ (fm)	J/A (MeV fm^3)	σ_R (mb)
587	U_4	0.2634	31.31	−123.77	1.53	0.86	1.62	0.88	1.79	0.90	1.43	94.8	92.0
587	U_s	0.2634	42.86	−169.42	1.53	0.85	1.49	0.86	1.53	0.87	1.43	130.0	92.9
587	U_s	0.2675	40.96	−160.60	1.26	0.88	1.38	0.90	1.62	0.92	1.45	126.8	92.8
1000	U_4	0.2860	27.80	−156.19	1.29	0.97	1.96	0.97	1.85	0.98	1.53	94.5	109.7
1000	U_s	0.2860	44.42	−249.59	1.30	0.96	2.14	0.94	1.75	0.95	1.53	151.0	110.8
1000	U_s	0.2880	40.41	−243.07	1.24	0.98	1.87	0.98	1.63	0.98	1.54	138.7	110.9
1050	U_4	0.2973	47.22	−126.90	1.34	1.08	0.91	1.08	0.86	1.08	1.58	170.0	105.0
1050	U_s	0.2973	76.70	−206.09	1.46	1.07	1.42	1.00	1.12	0.98	1.58	276.1	105.1
1050	U_s	0.3031	68.01	−187.60	1.46	1.14	1.28	1.19	0.93	1.19	1.61	252.3	104.9
1050	U_4	0.2860	27.80	−156.19	1.41	1.10	9.32	1.02	9.08	0.97	1.53	94.5	109.4

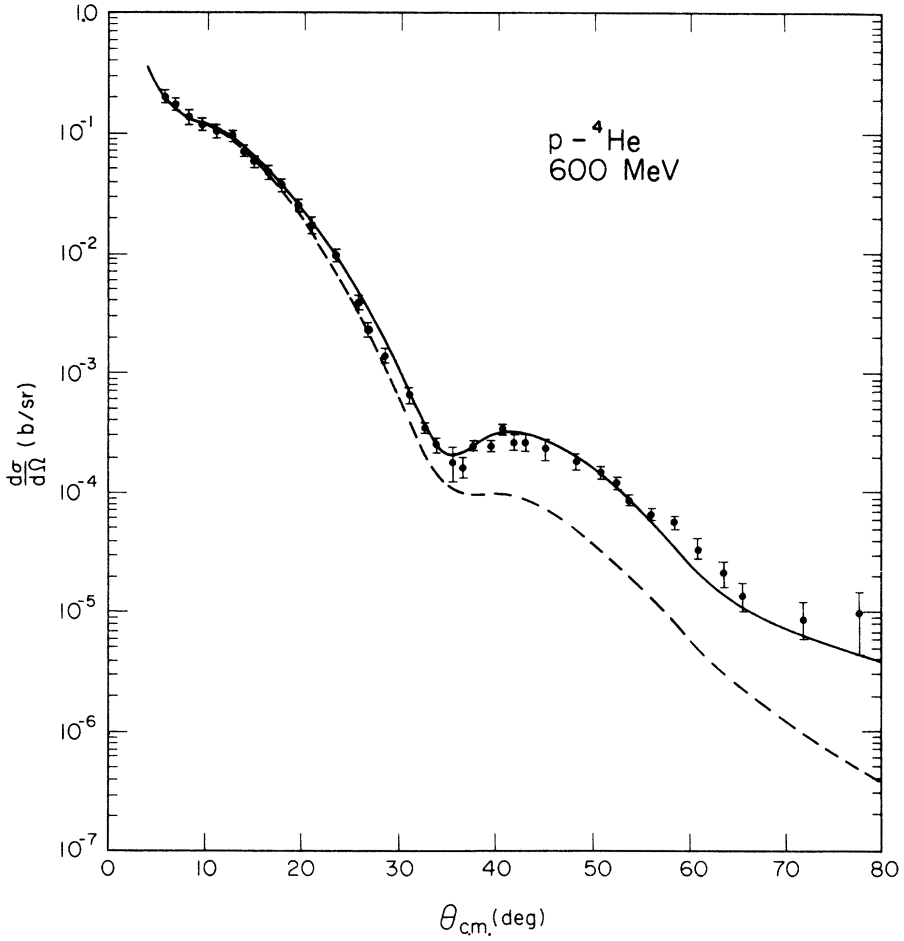

FIG. 1. The full curve is the result of using Eq. (1) for the optical model potential for 600 MeV p-^{4}He elastic scattering. The dashed curve is the result of using Eq. (4). Potentials of the U_4 type are used. The experimental data are from Ref. 1, and the curves have been scaled by the λ obtained in fitting to these data.

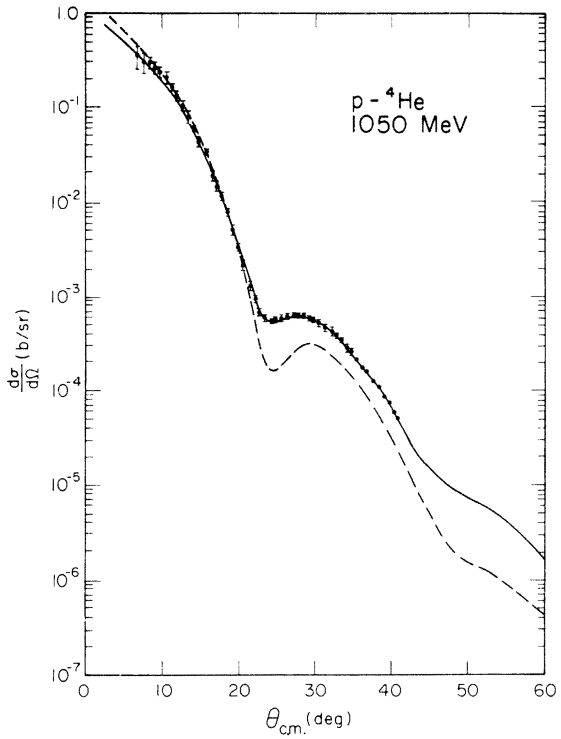

FIG. 2. The full curve is the result of using Eq. (1) for the optical model potential for 1050 MeV p-^{4}He elastic scattering. The dashed curve is the result of using Eq. (4). Potentials of the U_4 type are used. The experimental data are from Ref. 3, and the curves have been scaled by the λ obtained in fitting to these data.

only the small angle data, $|t| \leq 0.2$. The results are given in Table III, and show that reasonable fits are obtained for small $|t|$. As before, density A, which has the smaller rms radius, gives somewhat better fits to the data. The calculated χ^2/d.f. for $|t| \leq 0.4$, and that for all data, are not good. We next attempt to find a good fit to all of the data. The results are shown in Table IV for density A. We find that this procedure also yields reasonable χ^2/d.f. for $|t| \leq 0.2$, but the overall agreement with experiment, as indicated by the large χ^2/d.f. for the larger ranges of $|t|$, is poor. The results in Tables III and IV show that varying only V and W is not sufficient to produce reasonable fits to the data in the region of and beyond the diffraction dip. To the extent that Eqs. (1) and (4) can be identified, the predictions from V and W for α and σ_T are considerably different from their experimental values.

We now turn to a completely phenomenological analysis in which both the strength parameters and the geometry of the optical potential are allowed to vary. We use the parabolic Fermi shape function and initially fix c at 1.008 fm and w at 0.445, the values given by Frosch *et al.*[11] The diffusivity parameter z is then varied along with the strength parameters V and W to obtain good agreement with each of the experiments. The results are given in Table V and Figs. 1 and 2. Five parameter searches in which c and w were also allowed to vary did not give χ^2/d.f. appreciably different from those in Table V; further, the values of J/A and the rms radii were essentially unchanged. This suggests that, as in low energy analyses, the rms radius and volume integral are well determined by the data at each energy.

Results for optical potentials of both the U_s and U_4 types are given in Table V. Equivalent acceptable fits to the data are obtained for each type. In addition the U_s potentials determined from an E/m scaling of the U_4 potentials give acceptable fits to the data. The rms radius is quite insensitive to the type of potential used, and the volume integrals for U_s and U_4 exhibit almost the same E/m scaling as the strengths.

The substantial differences between the Brookhaven data at 1000 MeV and the Saclay data at 1050 MeV in the region of and beyond the first diffraction minimum result in a large change in the potential strength parameters over a relatively small energy interval. This result is independent of the assumed absolute normalization of the 1050 MeV cross section, a fact we have ascertained both by relaxing the absolute cross section constraint in the data fitting, and by maintaining this constraint but altering the quoted cross sections by a constant factor. The last row in Table V shows the results of a cross section calculation at 1050 MeV using the potential parameters from the 1000 MeV data. The χ^2/d.f. of this calculation is reasonable for $|t| \leq 0.2$, but deteriorates appreciably in the region

TABLE VI. Results of calculations with a U_4 potential where z was varied to improve the fit for $|t| \leq 0.2$ (GeV/c)^2.

T (MeV)	z (fm)	V (MeV)	W (MeV)	$\|t\| \leq 0.2$ (GeV/c)^2 χ^2/d.f.	λ	$\|t\| \leq 0.4$ (GeV/c)^2 χ^2/d.f.	λ	All data χ^2/d.f.	λ	J/A (MeV fm^3)	$\langle r^2 \rangle^{1/2}$ (fm)	σ_R (mb)
587	0.2734	31.31	−123.77	0.38	0.87	1.36	0.88	2.99	0.93	99.8	1.47	97.2
1000	0.2910	27.80	−156.19	1.10	1.00	1.87	0.98	2.12	1.00	96.9	1.55	113.0
1050	0.3023	47.22	−126.90	0.81	1.12	0.84	1.08	2.01	1.23	174.5	1.60	107.9

$0.2 \leq |t| \leq 0.4$. Further deterioration of the fit for $|t| \geq 0.4$ is not nearly so pronounced. Thus, the change in the potential strength parameters reflects the differences between the data sets in the region of the first diffraction minimum and subsequent maximum. The differences in the data in the region beyond $|t| \leq 0.4$ are not nearly as important.

Another feature that can be seen from Table V is that the χ^2/d.f. for $|t| \leq 0.2$ is greater than 1 for every case. We attempted to improve the small angle fit without destroying the acceptable χ^2/d.f. for all data, but were unable to accomplish an improvement. As an example, the results of one series of calculations for U_4 are given in Table VI. While the small angle data is quite well represented, the rest of the fit suffers. One point to notice, however, is that the improvement was obtained with a change in z of only 0.01 fm. Thus, the rms radii and volume integrals are essentially unchanged from the overall best fit values.

DISCUSSION

For any single energy we have shown that it is possible to obtain a reasonable fit to the small angle data using the shape parameters obtained from electron scattering and allowing the strength parameters to vary. When all of the data at a given energy are considered this is no longer possible. This is connected with the fact that in every case the rms radius of the potential is considerably smaller than the rms radius of the charge distribution.

The average of the rms radii determined by the analyses with U_s and U_4 potentials at each of the three energies is 1.52 ± 0.06 fm, a result which is in agreement with value 1.42 ± 0.05 fm for the rms radius of the proton matter distribution of ^{4}He obtained from the low energy electron scattering results of Frank *et al.*[12] The average rms radius obtained here is substantially smaller than the value 2.055 fm obtained by Satchler *et al.*[16] and the value 1.86 fm obtained by Thompson, Epstein, and Sawada[17] from analyses with $T_p \lesssim 50$ MeV. Thus, it appears that the rms radius of the p-^{4}He optical potential is energy dependent. In this regard, however, it should be noted that the rms radii given in Table V show a slight tendency to increase with increasing energy.

The volume integral per nucleon of the real central potential does not exhibit a smooth energy dependence. The values of J/A at 600 and 1000 MeV are essentially equal, while the value of J/A at 1050 MeV is larger by a factor of 1.8. This substantial change in the volume integral over such a small energy range is particularly remarkable in view of the negligible changes in the rms radius and the calculated reaction cross sections. As discussed above, the differences between the 1000 and 1050 MeV data in the region of the diffraction dip and subsequent maximum are responsible for most of the differences between the optical potentials at these energies. These differences persist in the volume integral of the real central potential, which, as an integrated quantity, is expected to be well determined by analyses of this type.

ACKNOWLEDGMENTS

We acknowledge computing support from the Instruction and Research Computing Center, The Ohio State University. One of us (BCC) acknowledges helpful conversations with Professor Bernard Mulligan, and the technical assistance of Ms. Annamarie Saggio. We thank Professor R. Beurtey, Professor D. Garreta, Professor K. Gotow, Professor G. Igo, and Professor J. Saudinos for very helpful communications and conversations regarding their experimental work.

---

*Supported in part by the National Science Foundation under the grant MPS-73-05103.

[1]E. T. Boschitz, W. K. Roberts, J. S. Vincent, M. Blecher, K. Gotow, P. C. Gugelot, C. F. Perdrisat, L. W. Swenson, and J. R. Priest, Phys. Rev. C 6, 457 (1972).

[2]H. Palevsky, J. L. Friedes, R. J. Sutter, G. W. Bennett, G. J. Igo, W. D. Simpson, G. C. Phillips, D. M. Corley, N. S. Wall, R. L. Stearns, and B. Gottschalk, Phys. Rev. Lett. 18, 1200 (1967).

[3]S. D. Baker, R. Beurtey, G. Bruge, A. Chaumeaux, J. M. Durand, J. C. Faivre, J. M. Fontaine, D. Garreta, D. Legrand, J. Saudinos, J. Thirion, R. Bertini, F. Brochard, and F. Hibou, Phys. Rev. Lett. 32, 839 (1974). A tabulation of the data which differs in some respects from the published data was provided by R. Beurtey (private communication). We use this tabulation of the data in the analysis reported here. We have also analyzed the published data, and find that no significant changes in the optical potential parameters are required.

[4]B. C. Clark, R. L. Mercer, D. G. Ravenhall, and A. M. Saperstein, Phys. Rev. C 7, 466 (1973).

[5]D. W. Rule and Y. Hahn, Phys. Rev. Lett. 34, 332 (1975).

[6]E. Lambert and H. Feshbach, Ann. Phys. (N.Y.) 76, 80 (1973). See also E. Boridy and H. Feshbach, Phys. Lett. 50B, 433 (1974).

[7]S. A. Gurvits, Y. Alexander, and A. S. Rinat, Phys. Lett. 59B, 22 (1975).

[8]G. W. Greenless, G. J. Pyle, and Y. C. Tang, Phys. Rev. 171, 1115 (1968).

[9]W. T. H. van Oers and Huang Haw, Phys. Lett. 45B, 227 (1973); W. T. H. van Oers, Huang Haw, N. E. Davison, A. Ingemarsson, B. Fagerström, and G. Tibell, Phys. Rev. C 10, 307 (1974).
[10]H. Feshbach, A. Gal, and J. Hüfner, Ann. Phys. (N.Y.) 66, 20 (1971).
[11]R. F. Frosch, J. S. McCarthy, R. E. Rand, and M. R. Yearian, Phys. Rev. 160, 874 (1967).
[12]H. Frank, D. Haas, and H. Prange, Phys. Lett. 19, 391, 719 (1965).
[13]D. V. Bugg, D. C. Salter, G. H. Stafford, R. F. George, K. F. Riley, and R. J. Tapper, Phys. Rev. 146, 980 (1966). Linear extrapolation gives $\sigma_{pp} = 47.51$ mb, $\sigma_{pn} = 40.32$ mb for the total cross sections at 1.696 GeV/c incident lab momentum. The averaged total cross section used is $\sigma_T = 43.91$ mb.
[14]L. M. C. Dutton, R. J. W. Howells, J. D. Jafar, and H. B. van der Raay, Phys. Lett. 25B, 245 (1967). They give $\alpha_p = 0.1 \pm 0.16$ and $\alpha_n = -0.50 \pm 0.15$ at 1.69 GeV/c incident lab momentum for the ratio of real to imaginary parts of the proton-proton and proton-neutron scattering amplitudes, respectively. The average ratio is then -0.2, but this may not be a very well determined quantity.
[15]An absolute normalization error of 20% was reported for the 600 and 1000 MeV cross sections. As the overall absolute normalization of the 1050 MeV data was rather arbitrary (Ref. 3), we choose to use 20% for it also.
[16]G. R. Satchler, L. W. Owen, A. J. Elwyn, G. L. Morgan, and R. L. Walter, Nucl. Phys. A112, 1 (1968).
[17]G. E. Thompson, M. B. Epstein, and T. Sawada, Nucl. Phys. A142, 571 (1970).